Nucl. Phys. B 1018 (2025) 116981

Contents lists available at ScienceDirect

Nuclear Physics, Section B

journal homepage: www.elsevier.com/locate/nuclphysb

High Energy Physics – Theory

D-brane and exponential potentials inspire warm inflation and swampland conjecture

Shama Sadiq [a], Nadeem Azhar [b,c], N. Myrzakulov [d,e], S. Toktarbay [d], A. Muratkhan [d], Sanjar Shaymatov [f,g,h], Abdul Jawad [a,i,*]

[a] Department of Mathematics, COMSATS University Islamabad, Lahore-Campus, Lahore-54000, Pakistan
[b] Department of Mathematics, National University of Modern Languages (NUML), Lahore Campus, Lahore-54000, Pakistan
[c] Research Center of Astrophysics and Cosmology, Khazar University, Baku AZ1096, 41 Mehseti Street, Azerbaijan
[d] Institute for Experimental and Theoretical Physics, Al-Farabi Kazakh National University, 050040, Almaty, Kazakhstan
[e] L. N. Gumilyov Eurasian National University, Astana 010008, Kazakhstan
[f] New Uzbekistan University, Movarounnahr Str. 1, Tashkent 100000, Uzbekistan
[g] University of Tashkent for Applied Sciences, Str. Gavhar 1, Tashkent 100149, Uzbekistan
[h] Western Caspian University, Baku AZ1001, Azerbaijan
[i] Institute for Theoretical Physics and Cosmology, Zhejiang University of Technology, Hangzhou 310023, China

ARTICLE INFO

Editor: Stephan Stieberger

ABSTRACT

This research explores the rapid expansion period of the early universe by applying the Chaplygin gas model, an alternative cosmological framework, to analyze the dynamics of inflationary processes. This study assesses the compatibility of three widely studied scalar field potentials with the latest observational constraints derived from the Planck datasets. Our analysis includes inflationary parameters such as slow-roll parameters, scalar power spectrum $\mathcal{P}_{\mathcal{R}}$, scalar spectral index n_s, dissipative ratio R, tensor-to-scalar ratio r and running of the scalar spectral index $\frac{dn_s}{d\ln k}$, within the theoretical frameworks of canonical scalar field dynamics and the Chaplygin gas cosmological model. These parameters help to paint a comprehensive picture of the inflationary epoch and its impact on the observable Universe. We also address the generalized ratio of the swampland de-Sitter conjecture through the expression of $\frac{T'V}{V'T}$ for three different potentials. We analyze inflation driven by a scalar field ϕ with decay rate $\Gamma(\phi,T)=C_\phi\frac{T^a}{\phi^{a-1}}$, where C_ϕ is a dimensionless coupling and a controls dissipation strength. Working in the strong dissipative regime ($R\gg 1$), we systematically investigate the background evolution and perturbation spectrum, deriving inflationary observables.

1. Introduction

The expanding universe concept originated with Georges Lemaître in the 1920s through theoretical work on general relativity. Edwin Hubble later confirmed this expansion observationally in the late 1920s-1930s. Hubble observed that distant galaxies are

* Corresponding author.
E-mail addresses: shamayasmeen36@gmail.com (S. Sadiq), nadeemazharsaeed@gmail.com, nadeem.azhar@numl.edu.pk (N. Azhar), nmyrzakulov@gmail.com (N. Myrzakulov), saken.yan@yandex.com (S. Toktarbay), arai12@mail.ru (A. Muratkhan), sanjar@astrin.uz (S. Shaymatov), abduljawad@cuilahore.edu.pk (A. Jawad).

https://doi.org/10.1016/j.nuclphysb.2025.116981
Received 13 April 2025; Received in revised form 28 May 2025; Accepted 8 June 2025

Available online 13 June 2025

receding from us, with their recessional velocity increasing with distance. This proportionality, formalized as Hubble's Law, provides direct evidence for cosmic expansion. This profound implication suggests that the universe was once much smaller and denser, a state referred to as the Big Bang. These observations establish the Big Bang paradigm as the standard model of cosmic evolution, from initial conditions to present-day expansion. These observations establish the Big Bang paradigm as the standard model of cosmic evolution, from initial conditions to present-day expansion. The expansion of the universe has also yielded significant insights into its nature and composition [1].

Observations of distant super-novae [2], gravitational lensing (GL) [3] and cosmic microwave background (CMB) [4] radiation have led to the understanding that the universe undergoes accelerated expansion, not merely constant growth. This acceleration is attributed to a mysterious force called dark energy [5], which appears to counteract the gravitational pull of matter and push galaxies apart at an increasing rate. However, the expansion of the universe is a fascinating phenomenon that not only reshaped our understanding of cosmology but also continues to provide valuable insights into the nature, composition, and ultimate destiny of the cosmos. Inflationary theory suggests that the universe underwent an extremely rapid, exponential expansion in the earliest fractions of a second following the Big Bang. Inflationary theory was developed to address certain issues with the standard big bang model, such as the monopole problem [6,7], flatness problem, homogeneity problem [8] and the horizon problem.

The horizon problem emerges from the observed thermal equilibrium between causally disconnected regions of the universe - areas that, according to standard cosmology, could never have achieved temperature uniformity through conventional thermal processes [9]. The inflationary paradigm suggests a phase of superluminal spatial growth in the universe's primordial stages, allowing distant regions to come into contact and reach thermal equilibrium before inflation ended. This resolves the horizon problem by ensuring that regions of the universe that were once in causal contact remain in thermal equilibrium. The geometry of the universe (whether it is flat, open, or closed) is described by the curvature parameter, which observations indicate is very close to flat. Without inflation, the early universe would need to be fine-tuned to an incredibly precise degree to remain flat over time. Inflation naturally drives the curvature parameter towards unity, making the universe flat on large scales. This resolves the flatness problem by explaining why the universe appears to be so close to flatness without requiring fine-tuning [9].

The homogeneity problem concerns the uniformity of the CMB radiation [7]. Large-scale observations reveal remarkable uniformity in the universe's matter distribution and physical properties across all directions. Without inflation, achieving this level of uniformity would require a mechanism for the early universe to quickly reach thermal equilibrium, which is not readily apparent in the standard Big Bang model. Inflationary theory provides a solution by exponentially expanding the universe, thereby smoothing out any irregularities in the density distribution and ensuring uniformity [10]. Grand unified field theories (GUTs) necessarily imply the generation of magnetic monopoles during high-energy phase transitions, hypothetical particles with isolated magnetic charges. If these particles were produced in the early universe as predicted by GUTs, they should be very abundant, which contradicts current observations. Inflationary theory resolves the monopole problem by predicting that the rapid expansion of the universe would dilute the density of these monopoles to extremely low levels.

The terms commonly associated with cosmological models that attempt to explain the inflationary epoch are cold and warm inflation [11]. The cold inflation scenario unfolds through two distinct mechanisms: an initial slow-roll period of accelerated cosmic expansion, followed by a reheating phase that restores thermal equilibrium [12]. Dissipation, or energy loss, is a crucial aspect of the system but is often overlooked in cold inflation models. Reheating is essential at the end of inflation to align the inflationary model with the big bang theory. Inflation, a key concept in cosmology, explores the dynamics of the early universe with significant dissipative effects [13]. Unlike cold inflation, which ignores dissipative processes, warm inflation incorporates interactions between the inflation field and other particles. In warm inflation, dissipative effects gradually convert the energy of the inflation field into radiation, transitioning the universe from accelerated expansion to radiation domination. This transition involves the decay of the inflation field into radiation particles, which influences the subsequent evolution of the universe. Warm inflation introduces unique consistency relations, which are crucial for testing theoretical models against observations and enhancing our theoretical framework for early universe physics [14].

Swampland distance/de Sitter conjectures [15,16] impose nontrivial restrictions on K-essence Lagrangian reconstructions in effective field theory. These criteria challenge the Einstein's gravity and the principles of string theory. One conjecture suggests that the inflation field should be constrained by the Planck mass, specifically $\Delta\phi \leq m_p$, or alternatively, $\Delta\phi \leq cm_p$, where c depends on the nature of the field. A further swampland conjecture constrains the scalar potential's gradient through the inequality $|\nabla_\phi V| \geq c.\frac{V}{m_p}$, where c is an $O(1)$ constant. This condition severely restricts inflationary scenarios—either preventing slow-roll inflation entirely or limiting it to sub-Planckian field excursions, depending on c's magnitude. The conjecture further connects to cosmological slow-roll parameters $\epsilon = \frac{1}{2}\left(\frac{V_\phi}{V}\right)^2$ and $\eta = \frac{V_{\phi\phi}}{V}$ (where $V_{\phi\phi} = \frac{d^2V}{d\phi^2}$), which quantify the field's dynamical evolution during inflation. Inflation takes place if $\eta \ll 1$ and $\epsilon \ll 1$.

The Chaplygin gas (CG) model [17], though first proposed in non-cosmological contexts, has gained significant attention in modern cosmology due to its unique negative pressure behavior. When applied to the Friedmann-Lemaître-Robertson-Walker (FLRW) framework in general relativity, CG offers a theoretical lens to analyze the universe's evolutionary dynamics under the influence of an exotic fluid. Unlike conventional models, CG distinguishes itself through a dynamically evolving equation of state (EoS), enabling novel interpretations of cosmic expansion [18,19]. Investigations into modified gravity theories have further expanded its applicability [20], though persistent limitations in modeling large-scale structure formation and reconciling the cosmological power spectrum remain unresolved [21]. To address these issues, Bento et al. [22] developed the generalized Chaplygin gas (GCG) model, which has emerged as a promising candidate for unifying dark energy and dark matter phenomena. Observational studies [23]-[24] increasingly

support the GCG framework, particularly its capacity to explain cosmic acceleration through a single fluid characterized by an unconventional EoS [25]. This unification of dark sector components underscores the GCG model's potential to simplify cosmological paradigms. The detailed analysis of inflation are also given in the literature [26–42].

In recent years, warm inflation has gained attention as a viable alternative to cold inflation, offering a mechanism where the inflaton's energy dissipates into a thermal bath during inflation. Unlike the standard scenario, this process allows a smooth transition to the radiation-dominated era, potentially avoiding the need for a separate reheating phase. This property also makes warm inflation promising in light of the swampland conjectures, which challenge the flatness and field range assumptions of traditional slow-roll models. In this work, we explore warm inflation within the GCG framework, which provides a unified description of dark energy and dark matter through an exotic fluid with a variable equation of state. We consider three types of scalar field potentials (D-brane for $p=2$, $p=4$ and exponential tail potentials) and examine their dynamics under a generalized dissipative coefficient. Specifically, we analyze key inflationary parameters by considering the dissipation coefficient $\Gamma(\phi,T)=C_\phi\frac{T^a}{\phi^{a-1}}$. Our study explores (i) the primordial curvature power spectrum $\mathcal{P}_\mathcal{R}$, (ii) scalar spectral index n_s, (iii) dissipation ratio $R=\frac{\Gamma}{3H}$, (iv) tensor-scalar ratio r and (v) the running $\frac{dn_s}{d\ln k}$ of the spectral index. Furthermore, we present graphical representations of the relationships between n_s-r, n_s-R as well as $n_s-\frac{dn_s}{d\ln k}$. Additionally, we examine the generalized ratio of the swampland de Sitter conjecture through the expression $\frac{T'V}{V'T}$.

The goal is to determine whether these setups yield inflationary observables consistent with Planck 2018 constraints and simultaneously satisfy the swampland de Sitter conjectures, thereby providing a theoretically motivated and observationally viable inflationary model. The structure of this manuscript is as follows: Section 2 includes a concise introduction to the warm inflationary paradigm is presented, alongside foundational principles of cosmological perturbation theory. We also explore the mathematical formulation of the GCG model is rigorously developed, emphasizing its EoS and implications for the unification of dark components. The D-Brane potential for $p=2$ is analyzed in Section 3, to derive inflationary observables and swampland conjectures supported by graphical representations of parameter trends. In Section 4, analytical expressions for inflationary parameters and swampland conjectures are derived within the D-Brane potential for $p=4$ framework. A novel potential with exponential tails is proposed and its inflationary dynamics are explored in Section 5. Finally, Section 6 demonstrates the key findings across all models are synthesized, emphasizing comparative insights into inflationary mechanisms and swampland criteria.

2. Generalized Chaplygin gas model

The CG [43] is an exotic fluid with unconventional thermodynamic properties, initially formulated by Sergei Chaplygin in the context of aerodynamics. Its defining feature is a non-linear inverse relationship between pressure p and energy density ρ, expressed via the EoS $p=-\frac{C_1}{\rho}$ where $C_1>0$ is a proportionality constant. Unlike classical ideal gases, CG exhibits a negative pressure that dominates at high densities, a behavior linked to its capacity to mimic dark energy in cosmological frameworks. The CG dynamically transitions between matter-like ($p\approx 0$) and dark energy-like ($p\sim-\rho$) phases, enabling it to unify dark matter and dark energy phenomenology under a single fluid description. This model is originally derived to study lift forces in fluid dynamics, CG has been reinterpreted in cosmology to address cosmic acceleration, structure formation, and the late-time expansion of the universe. The EoS's inherent negative pressure violates the strong energy condition, allowing CG to mediate repulsive gravitational effects while retaining clustering properties akin to cold dark matter.

The GCG model was originally proposed to unify dark matter and dark energy phenomena in the late-time universe [24]. In the present study, however, we do not treat the GCG as a physical fluid but rather as a geometric modification to the background cosmology through its influence on the Friedmann equation. This approach introduces a nonlinear dependence on the scalar field energy density, effectively modifying the expansion dynamics during the inflationary phase. As a result, the evolution of the Hubble parameter is slowed, which aids in sustaining the inflationary process. It is worth emphasizing that our formulation does not require the Chaplygin gas to exist as a thermodynamic component during inflation. Instead, consistent with interpretations found in the literature, we adopt the GCG as a structural modification to the cosmological background geometry, applicable even in early-universe scenarios. Meanwhile, the radiation component intrinsic to warm inflation arises independently due to dissipative processes involving the scalar field. Hence, the radiation bath and inflaton field evolve on a background governed by GCG-modified gravity, without assuming any physical coupling to the Chaplygin gas. This enhanced model incorporates additional degrees of freedom through a parameterized equation of state

$$p=-\frac{C_1}{\rho^\alpha},\quad \text{where}\quad 0<\alpha\leq 1. \tag{2.1}$$

Notably:

- When $\alpha=1$, the GCG exactly reduces to the standard CG model.
- For intermediate values ($0<\alpha<1$), the model exhibits quintessence-like characteristics.
- As α approaches 0, it demonstrates phantom-like properties.

The corresponding energy density evolution emerges naturally from the conservation equation

$$\rho=\left(C_1+\frac{C_2}{a^{3(1+\alpha)}}\right)^{\frac{1}{1+\alpha}}, \tag{2.2}$$

where a is the scale factor and C_2 an integration constant. This elegant formulation allows the GCG to smoothly interpolate between dust-like behavior at early times ($a \ll 1$) and dark energy dominance at late times ($a \gg 1$). In this context, the term proportional to a^{-3} as the energy density of matter ρ_m is achieved.

Building upon Eq. (2.2), we generalize the energy density formulation to incorporate both conventional matter and scalar field contributions. The complete energy density expression becomes

$$\rho = \left(C_1 + \rho_m^{1+\alpha}\right)^{\frac{1}{1+\alpha}} \rightarrow \left(C_1 + \rho_\phi^{1+\alpha}\right)^{\frac{1}{1+\alpha}} \tag{2.3}$$

where the left term represents the original GCG form for matter density ρ_m while the right term extends this to include the scalar field energy density $\rho_\phi = \frac{1}{2}\dot{\phi} + V(\phi)$. The parameter α maintains its original constraints ($0 < \alpha \leq 1$). We interpret the theoretical framework as a non-covariant modification of gravity, where Eq. (2.3) is not derived from Eq. (2.2). Instead, following the formalism in [17], Eq. (2.3) independently defines a modified Friedmann equation. To contextualize this, we analyze a spatially flat universe dominated by two components: (i) A self-interacting inflationary scalar field. (ii) A relativistic radiation fluid. Within this configuration, the modified Friedmann equation can be expressed as

$$H^2 = \frac{1}{3}((C_1 + \rho_\phi^{1+\alpha})^{\frac{1}{1+\alpha}} + \rho_\gamma). \tag{2.4}$$

In this manuscript, we consider $M_p^2 = 1$.

The modified Friedmann equation (Eq. (2.4)) originates from a non-covariant gravitational modification, yet remarkably preserves diffeomorphism invariance in (3+1) dimensions [44]. This crucial feature maintains total stress-energy conservation while allowing for novel cosmological dynamics.

2.1. Warm inflation framework with generalized Chaplygin gas background

Warm inflation presents an attractive alternative to the standard cold inflation scenario by incorporating dissipative effects through which the inflaton field continuously transfers energy into a thermal radiation bath. This leads to a radiation-dominated environment that coexists with inflation, eliminating the need for a distinct reheating phase. One of the key features of warm inflation is that it allows for sustained inflationary dynamics via thermal friction, which slows down the motion of the scalar field even when the potential is not extremely flat.

In our model, we consider a spatially flat Friedmann-Robertson-Walker (FRW) universe composed of a canonical scalar field ϕ and a radiation fluid ρ_γ. The cosmic expansion is governed by a modified Friedmann equation derived from the GCG model

$$H^2 = \frac{1}{3}\left(\sqrt{C_1 + V^2(\phi)} + \rho_\gamma\right), \tag{2.5}$$

where C_1 is a positive integration constant and $V(\phi)$ is the scalar potential. During the inflationary phase, the energy density of the scalar field dominates over radiation ($\rho_\phi \gg \rho_\gamma$), and equation (2.5) simplifies to

$$H^2 \approx \frac{1}{3}\sqrt{C_1 + V^2(\phi)}. \tag{2.6}$$

Compared to the standard Friedmann equation, this GCG-based modification results in a more slowly varying Hubble parameter, which contributes to extending the inflationary period and facilitates the realization of slow-roll conditions.

The scalar field evolves according to the equation

$$\ddot{\phi} + (3H + \Gamma)\dot{\phi} + V_\phi = 0, \tag{2.7}$$

where Γ is the dissipation coefficient, responsible for converting inflaton energy into radiation. The friction term $\Gamma\dot{\phi}$ slows the evolution of the scalar field, providing the physical mechanism for sustaining inflation even with steeper potentials.

We assume a generalized form of the dissipation coefficient:

$$\Gamma(\phi, T) = C_\phi T^a \phi^{a-1}, \tag{2.8}$$

where C_ϕ is a positive constant and a determines the strength and form of the dissipation. The temperature of the thermal bath T is derived self-consistently from the radiation energy density $\rho_\gamma = C_\gamma T^4$, where $C_\gamma = \frac{\pi^2 g_*}{30}$ and g_* is the number of relativistic degrees of freedom. Combining with the slow-roll equations, the temperature can be expressed as:

$$T = \left(\frac{V_\phi^2 \phi^{a-1}}{4C_\gamma H}\right)^{\frac{1}{4+a}}. \tag{2.9}$$

The efficiency of dissipation is quantified by the dimensionless ratio

$$R = \frac{\Gamma}{3H}, \tag{2.10}$$

which divides the dynamics into two regimes:

- **Weak dissipative regime:** $R \ll 1$
- **Strong dissipative regime:** $R \gg 1$

In this work, we focus on the strong dissipative regime. In this case, the friction term dominates over Hubble damping, and the scalar field equation (2.7) reduces under slow-roll conditions to:

$$3H(1+R)\dot{\phi} \approx -V_{\phi}. \tag{2.11}$$

This shows explicitly how a large R (i.e., strong dissipation) suppresses $\dot{\phi}$, thus enabling a slow-roll phase even for potentials that are not exceptionally flat.

To verify the viability of slow-roll inflation, we define the following slow-roll parameters [45]

$$\epsilon = \frac{1}{2}\left(\frac{V_{\phi}}{V}\right)^2, \quad \eta = \frac{V_{\phi\phi}}{V}, \quad \beta = \frac{\Gamma_{\phi}V_{\phi}}{\Gamma V}, \quad \sigma = \frac{V_{\phi}}{\phi V}. \tag{2.12}$$

For sustained warm inflation, these parameters must satisfy the extended conditions:

$$\epsilon, \eta, \beta, \sigma \ll 1 + R. \tag{2.13}$$

In our analysis, we demonstrate analytically and numerically that these conditions are fulfilled for physically motivated parameter choices, including $a = 0$ and $a = -1$, and realistic values of C_{ϕ}, κ, m, and α. This confirms that slow-roll inflation is dynamically supported in our framework due to the interplay between the GCG-modified background and the strong dissipative dynamics of the scalar field. In the next subsection, we present the perturbation theory relevant to warm inflation and derive expressions for observable quantities such as the scalar spectral index, tensor-to-scalar ratio, and running of the spectral index.

2.2. Cosmological perturbation

In warm inflation models, the presence of a thermalized radiation component with temperature T exceeding the Hubble rate ($T > H$) fundamentally alters the nature of primordial fluctuations. Unlike in cold inflation where quantum vacuum fluctuations dominate, the inflationary perturbations $\delta\phi$ in this scenario are primarily thermally induced. This thermal origin of fluctuations leads to a modified expression for the power spectrum of curvature perturbations, which incorporates both the temperature-dependent effects and the dissipative dynamics characteristic of warm inflation as [46]

$$\mathcal{P}_{\mathcal{R}}^{\frac{1}{2}} \simeq \left(\frac{H}{2\pi}\right)\left(\frac{3H^2}{V_{,\phi}}\right)(1+R)^{\frac{5}{4}}\left(\frac{T}{H}\right)^{\frac{1}{2}}. \tag{2.14}$$

The normalization convention aligns with standard cold inflation in the limit $R \to 0$, where the radiation temperature T becomes comparable to the Hubble parameter H. Meanwhile, the scalar spectral index n_s, which quantifies deviations from scale invariance in primordial fluctuations, is expressed within the leading-order slow-roll formalism as [46]

$$\begin{aligned} n_s &= 1 + \frac{d\ln P_R}{d\ln k}, \\ &\simeq 1 - \frac{(17+9R)}{4(1+R)^2}\epsilon - \frac{(1+9R)}{4(1+R)^2}\beta + \frac{3}{2(1+R)}\eta. \end{aligned} \tag{2.15}$$

The scale dependence of the primordial power spectrum is characterized by the running of the scalar spectral index, denoted as $\frac{dn_s}{d\ln k}$. This quantity, which measures the variation of the spectral index n_s with respect to logarithmic scale k, was first derived in [45] and plays a crucial role in testing inflationary models against precision observational data. The running parameter provides important constraints on the dynamics of the inflationary potential and its higher-order derivatives. It is defined as follows

$$\begin{aligned} \frac{dn_s}{d\ln_k} = -\frac{3}{4R^2}\Big(&6\beta^2 - 5\beta\eta + 6\beta\epsilon - 6\gamma\epsilon + 2\zeta^2 + 9\epsilon^2 \\ &- 4\eta\epsilon\Big). \end{aligned} \tag{2.16}$$

The second-order slow-roll parameters ζ^2 and γ, introduced to refine the dynamics of inflationary models under thermal and dissipative effects, are defined as [17]

$$\zeta^2 = \left(\frac{V_{,\phi}V_{,\phi\phi\phi}}{V^2}\right), \quad \gamma = \left(\frac{\Gamma_{,\phi\phi}}{\Gamma}\right). \tag{2.17}$$

The tensor-to-scalar ratio, denoted as r, serves as a fundamental observable in inflationary cosmology and is given as [46]

$$r = \left(\frac{H}{T}\right)\frac{16\epsilon}{(1+R)^{\frac{5}{2}}}. \tag{2.18}$$

When analyzing warm inflation scenarios with specific scalar potentials and dissipative coefficients, the background evolution can be effectively described using slow-roll parameters. In this work, we examine how a generalized power-law dependence of the inflation decay rate on both the scalar field and the thermal bath temperature T—affects inflationary dynamics for power-law plateau potentials. Our analysis focuses exclusively on the strong dissipation regime, where the condition $R \geq 1$ (or equivalently $\Gamma \geq 3H$) holds. For this regime, we adopt a generalized parametrization of the dissipative coefficient:

$$\Gamma(\phi, T) = C_\phi \frac{T^a}{\phi^{a-1}}. \tag{2.19}$$

Here, C_ϕ represents a dimensionless parameter encoding microscopic dissipative dynamics, while the exponent a characterizes the decay rate's scaling behavior. This parametrization allows systematic study of how different dissipative microphysics influence inflationary observables while maintaining analytical tractability. For this choice, the expression of thermal bath becomes

$$T = \left(\frac{V_{,\phi}^2 \phi^{a-1} C_\phi^{-1}}{4 C_\gamma H} \right)^{\frac{1}{(4+a)}}. \tag{2.20}$$

Next, we will construct inflationary parameters and swampland de-Sitter conjecture for well-known potentials.

3. D-brane ($p = 2$) model and inflationary parameters

In the D-brane framework, D-branes are extended objects in string theory, where p represents the spatial dimensions the brane occupies. For $p = 2$, the D_2-brane, the brane is a membrane that exists in three-dimensional space. The dynamics of D_2-branes are described by the Dirac-Born-Infeld (DBI) action, which governs their interaction with the background fields, such as the dilaton and the Ramond-Ramond fields. The potential energy associated with D_2-branes typically involves the contributions of tension and various fluxes threading through the brane. The potential of D-Brane model for $p = 2$ is given as [47]

$$V(\phi) = \Lambda^4 \left(1 - \left(\frac{m}{\kappa \phi} \right)^2 \right), \tag{3.1}$$

where Λ is free parameter and m is dimensionless parameter. By combining the Eq. (3.1) with the dissipation relation (Eq. (2.20)), we derive the temperature of the thermal bath as a function of the inflaton field

$$T = 3^{\frac{1}{a+4}} \left(\frac{m^4 \phi^{a-7} m_p^2}{\kappa^4 C_\gamma C_\phi \sqrt{C_1 + (1 - \frac{m^2}{\kappa^2 \phi^2})^2}} \right)^{\frac{1}{a+4}}. \tag{3.2}$$

Substituting the thermal bath temperature $T(\phi)$ into the general dissipation form $\Gamma(\phi, T) = C_\phi \frac{T^a}{\phi^{a-1}}$ yields

$$\Gamma = \left(3^{\frac{1}{a+4}} \left(\frac{m^4 \phi^{a-7} m_p^2}{\kappa^4 C_\gamma C_\phi \sqrt{C_1 + \left(1 - \frac{m^2}{\kappa^2 \phi^2}\right)^2}} \right)^{\frac{1}{a+4}} \right)^a \times \phi^{1-a} C_\phi. \tag{3.3}$$

The dissipative ratio R, takes the following form when we substitute our derived dissipation coefficient

$$R = \frac{\left(3^{\frac{1}{a+4}} \left(\frac{m^4 \phi^{a-7} m_p^2}{\kappa^4 C_\gamma C_\phi \sqrt{C_1 + \left(1 - \frac{m^2}{\kappa^2 \phi^2}\right)^2}} \right)^{\frac{1}{a+4}} \right)^a}{\sqrt{C_1 + \left(1 - \frac{m^2}{\kappa^2 \phi^2}\right)^2}} \times \phi^{1-a} C_\phi m_p^2. \tag{3.4}$$

For $R \gg 1$, the standard slow-roll conditions are modified to $\{\epsilon, \eta, \beta, \sigma\} \ll R$.

3.1. Cosmological perturbations

In the strong-dissipation limit where $R = \frac{\Gamma}{3H} > 1$, the scalar perturbation spectrum undergoes significant modification compared to conventional cold inflation scenarios. The power spectrum amplitude given by Eq. (2.14) transforms to

$$\mathcal{P}_{\mathcal{R}}^{\frac{1}{2}} \simeq \left(\frac{H}{2\pi}\right)\left(\frac{3H^2}{V_\phi}\right)\left(\frac{T}{H}\right)^{\frac{1}{2}} R^{\frac{5}{4}}. \tag{3.5}$$

By substituting all applicable expressions into Eq. (3.5), the equation transforms into

$$\begin{aligned}\mathcal{P}_{\mathcal{R}} = {} & \frac{\kappa^2\phi^3\left(C_1+\left(1-\frac{m^2}{\kappa^2\phi^2}\right)^2\right)^{3/2}}{36\pi m^2 m_p^6} \\ & \times \sqrt{\frac{3^{\frac{a+5}{a+4}} m_p^2 \left(\frac{m^4\phi^{a-7}m_p^2}{\kappa^4 C_\gamma C_\phi \sqrt{C_1+\left(1-\frac{m^2}{\kappa^2\phi^2}\right)^2}}\right)^{\frac{1}{a+4}}}{\sqrt{C_1+\left(1-\frac{m^2}{\kappa^2\phi^2}\right)^2}}} \\ & \times \left(\frac{\left(3^{\frac{1}{a+4}}\left(\frac{m^4\phi^{a-7}m_p^2}{\kappa^4 C_\gamma C_\phi \sqrt{C_1+\left(1-\frac{m^2}{\kappa^2\phi^2}\right)^2}}\right)^{\frac{1}{a+4}}\right)^a}{\sqrt{C_1+\left(1-\frac{m^2}{\kappa^2\phi^2}\right)^2}}\right)^{5/4} \\ & \times \phi^{1-a} C_\phi m_p^2. \end{aligned} \tag{3.6}$$

In the strongly dissipative regime, the scalar spectral index n_s acquires additional temperature-dependent terms compared to cold inflation scenarios. The generalized expression becomes

$$n_s = 1 - \frac{3}{R}(3\epsilon + 3\beta - 2\eta). \tag{3.7}$$

One can obtain the expression of n_s by substituting Eq. (3.4) into Eq. (3.7). Additionally, the expression of (ζ^2), γ, r and $\frac{dn_s}{dlnk}$ can also be found through straightforward calculations.

3.2. Swampland conjectures

The string theory landscape refers to the vast theoretical space of possible vacuum solutions arising from different compactifications in string theory, each characterized by distinct physical parameters [48]. This multidimensional parameter space encompasses:

- Various false vacuum configurations.
- Alternative compactification geometries.
- Multiple flux stabilization possibilities.

Complementing this landscape is the conceptual "swampland" - the set of effective field theories that, while internally consistent, cannot be ultraviolet-completed within string theory. To systematically distinguish between landscape-compatible theories and those relegated to the swampland, two fundamental conjectures have emerged:

- **Swampland Distance Conjecture:**

  Proposes that traversing large distances in field space necessarily introduces an infinite tower of exponentially light states. In the context of effective field theory (EFT), the range traversed by the scalar fields within the field space is subject to an upper bound as

  $$\frac{\Delta\phi}{M_p} \leq C_1,$$

  where C_1 is some constant of order of unity.
- **Swampland de Sitter Conjecture:**

  Suggests that stable de Sitter vacua may be inconsistent with quantum gravity, implying stringent constraints on positive cosmological constants. The scalar field potentials of any EFT should obey one of the following conditions [49–51]

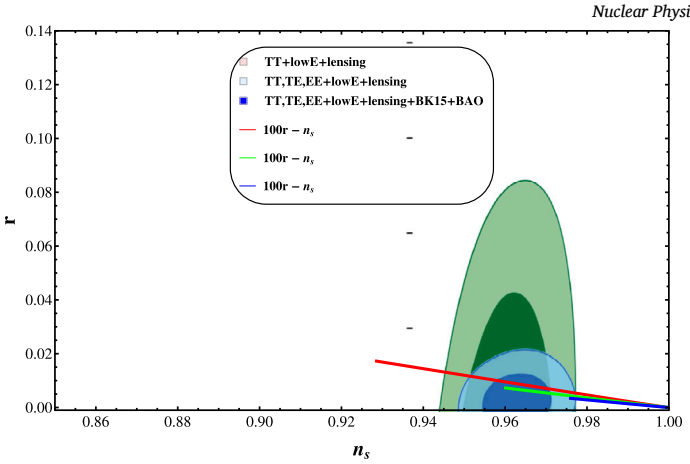

Fig. 1. Plot of r (ratio between tensor to scalar) against n_s scalar spectral index) for D-Brane ($p = 2$) model.

$$\frac{|\Delta V|}{V} \geq \frac{C_2}{M_p},$$

or

$$\frac{min(\nabla_i \nabla_j V)}{V} \leq -\frac{C_3}{M_p},$$

Here, C_2 and C_3 are dimensionless constants with values near 1. The operator ∇ denotes the field-space gradient, while $min(\nabla_i \nabla_j V)$ represents the smallest eigenvalue of the Hessian matrix $\nabla_i \nabla_j V$, evaluated in an orthonormal basis. In warm inflation, this conjecture adopts a modified form to account for

$$\begin{aligned}\frac{T'V}{V'T} = &\left(\kappa^6 \phi^{10-a} C_\gamma C_\phi \left(1 - \frac{m^2}{\kappa^2\phi^2}\right)\sqrt{C_1 + \left(1 - \frac{m^2}{\kappa^2\phi^2}\right)^2}\right.\\ &\times \left(\frac{(a-7)m^4\phi^{a-8}m_p^2}{\kappa^4 C_\gamma C_\phi \sqrt{C_1 + \left(1 - \frac{m^2}{\kappa^2\phi^2}\right)^2}}\right.\\ &\left.\left. - \frac{2m^6\phi^{a-10}m_p^2\left(1 - \frac{m^2}{\kappa^2\phi^2}\right)}{\kappa^6 C_\gamma C_\phi \left(C_1 + \left(1 - \frac{m^2}{\kappa^2\phi^2}\right)^2\right)^{3/2}}\right)\right)\\ &\times (2(a+4)m^6 m_p^2)^{-1}.\end{aligned}$$

If the ratio satisfies the condition $\frac{T'V}{V'T} < 1$, one can achieve the swampland conjectures [52].

3.3. Graphical part

This section analyzes the relationships between key inflationary observables and swampland criteria by plotting them against the n_s. The proposed inflationary framework is tested against modern astrophysical constraints, primarily leveraging measurements of cosmic microwave background (CMB) temperature anisotropies. Predictions of the model are evaluated on the $n_s - r$ plane, which features observational constraints derived from CMB data. Recent high-precision results from the Planck satellite experiments [53,54] provide stringent bounds on these parameters. To assess consistency with observations, we systematically investigate:

- The ratio between tensor to scalar r versus n_s.
- The dissipation ratio R versus n_s.
- The running $\frac{dn_s}{d\ln k}$ of the spectral index versus n_s.
- The thermal-to-adiabatic ratio $\frac{VT'}{TV'}$ versus n_s.

- **Behavior of r against n_s:**
  For $R \gg 1$, we numerically evaluate the expression of r as a function of the scalar spectral index n_s using the theoretical framework established in Eqs. (2.18) and (3.7). Fig. 1 presents these cosmological predictions for three representative values of the dissipation

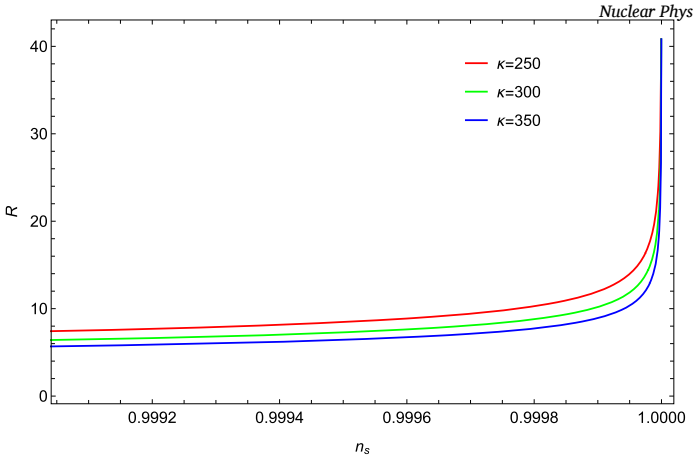

Fig. 2. Plot of $R = \frac{\Gamma}{3H}$ against n_s for D-Brane ($p = 2$) model with $a = 0$.

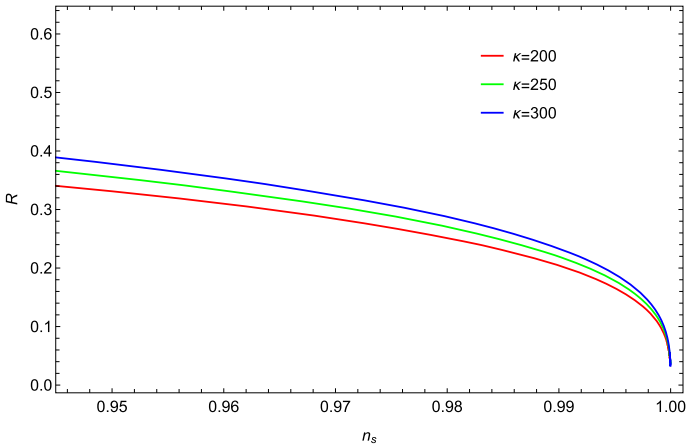

Fig. 3. Plot of $R = \frac{\Gamma}{3H}$ against n_s for D-Brane ($p = 2$) model with $a = 1$.

parameter $\kappa = 160,\ 200,\ 240$, while maintaining fixed values for other key parameters: $C_\gamma = 70$, $M_p = 1$ (in natural unit), $C_1 = 10^{-45}$, $m = 15$, $\alpha = 500$ and $C_\phi = 8.5$. Our analysis reveals a consistent decreasing trend in r across the observationally relevant range of n_s, with all computed trajectories satisfying the latest Planck collaboration constraints of $n_s = 0.9649 \pm 0.0042$ and $r < 0.066$ at 95% confidence level [53,54]. The results demonstrate particular sensitivity to the dissipation parameter κ, with variations of $\pm 20\%$ producing distinct but observationally viable curves. This systematic behavior confirms the robustness of the GCG framework within current observational bounds, suggesting that strong dissipative effects preferentially suppress tensor modes relative to scalar perturbations. The successful agreement with Planck data across our parameter choices indicates that the model requires no fine-tuning to remain consistent with measurements of the CMB.

- **Behavior of R against n_s:** Figs. 2 and 3 illustrate the relationship between the dissipative ratio $R = \frac{\Gamma}{3H}$ and the scalar spectral index n_s, derived from Eqs. (2.18) and (3.4), under two distinct scenarios: Fig. 2 ($a = 0$) and Fig. 3 ($a = 1$). For Fig. 2, the generalized dissipative coefficient $\Gamma(\phi, T) = C_\phi \frac{T^a}{\phi^{a-1}}$, simplifies to $\Gamma = C_\phi \phi$ when $a = 0$. Substituting this, the dissipative ratio becomes $R = \frac{C_\phi \phi}{3H}$. The analysis employs three values of the parameter $\kappa = 250,\ 300,\ 350$, with fixed constants $C_\gamma = 70$, $C_\phi = 8.5$ $\alpha = 500,\ m = 15$ and $M_p = 1$. In Fig. 3, the system is analyzed under the assumption of a strong dissipative regime with $a = 1$. Here, κ retains the same values (250, 300, 350), while parameters $C_\gamma = 70$, $C_\phi = 0.439$ $\alpha = 500$, $m = 15$ and $M_p = 1$ are held constant. The trajectories of n_s span $n_s \in [0.94,\ 0.99]$ across $R \in [0,\ 15]$. By enforcing the critical warm inflation condition $\frac{T}{H} > 1$, the analysis identifies the parameter space where the strong dissipative regime dominates.

- **Behavior of $\frac{dn_s}{d\ln k}$ and n_s:**
Recent analysis by the Planck 2018 collaboration has precisely measured the scale dependence of the scalar spectral index n_s, revealing a slightly negative running that is statistically consistent with zero. Our investigation explores this running through three distinct scenarios characterized by different values of the parameter $a = 0, 1, -1$, as illustrated in caption of Figs. 4–6. In

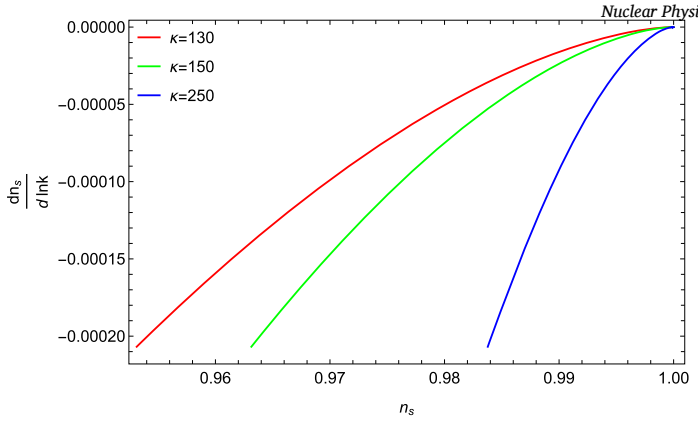

Fig. 4. Plot of running $\frac{dn_s}{dlnk}$ of the scalar spectral index against n_s (scalar spectral index) for D-Brane ($p=2$) model with $a=0$.

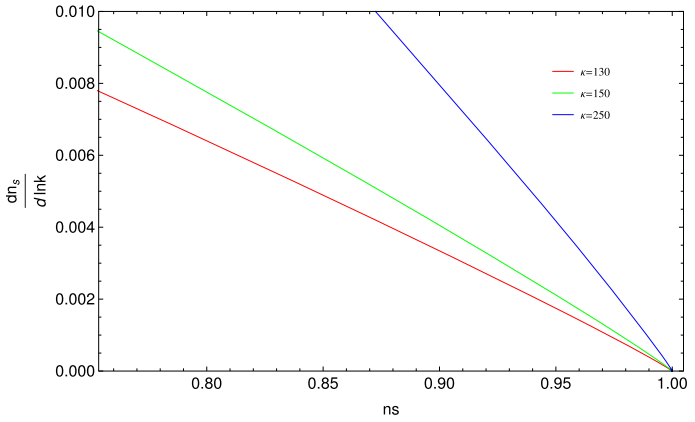

Fig. 5. Plot of running $\frac{dn_s}{dlnk}$ of the scalar spectral index against n_s (scalar spectral index) for D-Brane ($p=2$) model with $a=1$.

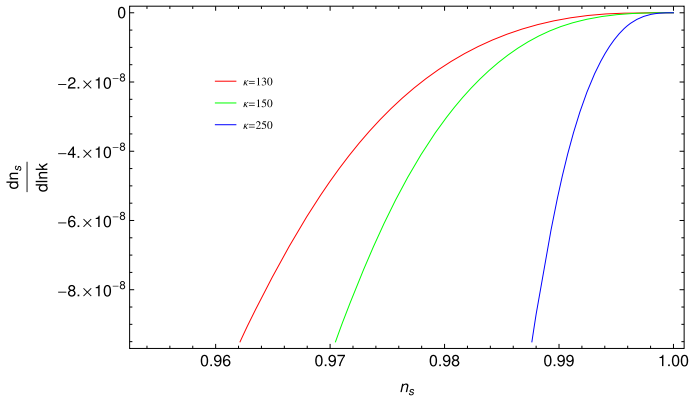

Fig. 6. Plot of running $\frac{dn_s}{dlnk}$ of the scalar spectral index against n_s (scalar spectral index) for D-Brane ($p=2$) model with $a=-1$.

Fig. 4 ($a=0$), we examine the scale dependence $\frac{dn_s}{dlnk}$ across three dissipation parameter values $\kappa = 130, 150, 250$, while holding other parameters fixed $C_\gamma = 70$ $M_p = 1$ $\alpha = 0.5$ $m = 13$ and $C_\phi = 5$. The results demonstrate excellent agreement with Planck's reported range $\frac{dn_s}{dlnk} = -0.0126^{+0.0098}_{-0.0087}$ within the observational window $n_s = 0.9649 \pm 0.0042$, confirming the physical consistency of this configuration [53,54].

Fig. 5 ($a=1$) presents an interesting contrast when analyzed under identical parameter choices. Here, the model generates positive running values $\frac{dn_s}{dlnk} > 0$, which are observationally disfavored and suggest potential limitations of this particular parameterization. However, the scenario recovers physical consistency in Fig. 6 ($a=-1$), where the predicted running again falls

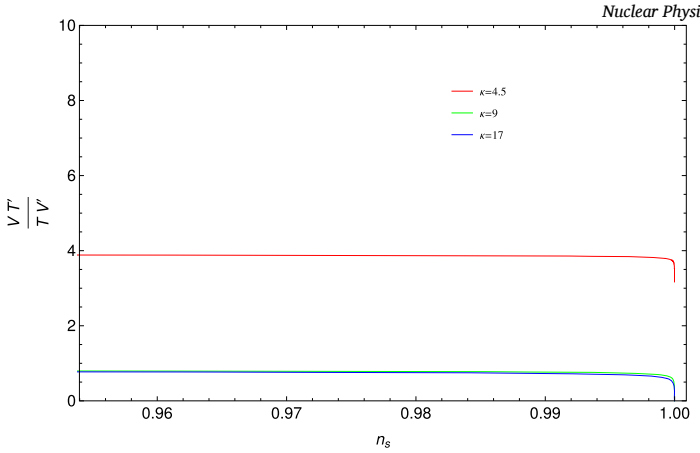

Fig. 7. Plot of $\frac{VT'}{TV'}$ versus n_s for exponential tails potential with $a = 0$.

within Planck's constraints, demonstrating the model's viability for certain parameter combinations [53,54]. These systematic comparisons reveal that the model's consistency with observational data depends sensitively on both the dissipation mechanism (through κ) and the specific form of the thermal coupling (through a). The successful agreement for $a = 0$ and $a = -1$ cases, contrasted with the unphysical $a = 1$ results, provides valuable insights into the parameter space where the GCG framework remains compatible with precision CMB measurements while maintaining its distinctive thermal characteristics.

- **Behavior of $\frac{VT'}{TV'}$ versus n_s:** Fig. 7 examines the relationship between the dimensionless parameter $\frac{VT'}{TV'}$, derived from the de Sitter conjecture and the scalar spectral index n_s, evaluated for three distinct values of κ. For $\kappa = 9,\ 17$, the ratio $\frac{VT'}{TV'}$ consistently remains below unity (< 1), satisfying the criteria of the swampland conjectures and confirming their validity under these conditions.

4. D-brane ($p = 4$) model

The D_4-brane ($p = 4$) extends through five spatial dimensions. The potential for D_4-branes also follows the DBI formalism, but the energy landscape becomes more complex due to the increased number of dimensions, leading to richer topological and gauge field structures. Both cases involve non-linear potentials that are sensitive to the geometry of the compactified extra dimensions and play a critical role in scenarios such as brane inflation, where the shape of the potential helps govern the dynamics of the early universe's evolution. Potential of this brane form is defined as follows [7]

$$V = \left(1 - \left(\frac{m}{k\phi}\right)^4\right).$$

By applying the same analytical methodology to this potential, we derived the expression of R, n_s, r, $\mathcal{P}_{\mathcal{R}}{}^{\frac{1}{2}}$ and $\frac{T'V}{TV'}$ and discussed their physical importance through plots in the upcoming section.

4.1. Graphical part

- **Behavior of r versus n_s:** In the case of D-Brane ($p = 4$) model, we present graphs illustrating the tensor-to-scalar ratio r and the scalar spectral index n_s in Fig. 8. We plot the trajectories for $\kappa = 450,\ C_\phi = 100,\ C_1 = 10^{-45},\ \alpha = 6 \times 10^5$ and $m = 90$. Analysis of the plotted results reveals that the scalar spectral index $n_s = 0.9649 \pm 0.0042$, consistent with the Planck collaboration's measured range, constrains the tensor-to-scalar ratio to $r < 0.066$ (68% confidence level). This agreement validates the consistency of our theoretical framework with the latest observational constraints, as shown in [53,54].

- **Behavior of R versus n_s:** The graph in Fig. 9 depicts the relationship between the scalar spectral index n_s and the dissipative ratio R for different values of κ. Fig. 9 analyzes the parameter space of the scalar spectral index n_s within the 68% confidence interval $0.94 \lesssim n_s \lesssim 0.99$, derived from observational constraints. Across this range, the dissipative ratio R consistently aligns with the theoretical requirements of the model, confirming its compatibility with the defined observational bounds.

- **Behavior of $\frac{dn_s}{d\ln k}$ versus n_s:** Our numerical analysis reveals key features of the spectral index running in strong dissipative regimes ($R \gg 1$), as illustrated in Figs. 10–12. These results explore three distinct thermal coupling scenarios ($a \in \{0, \pm 1\}$) across multiple dissipation scales (κ). Fig. 10 ($a = 0$) demonstrates remarkable consistency with observational constraints, showing $n_s \in [0.92, 0.98]$ and $\frac{dn_s}{d\ln k} \in (-0.0002, 0.0004)$. The tight clustering of running values near zero strongly supports the model's

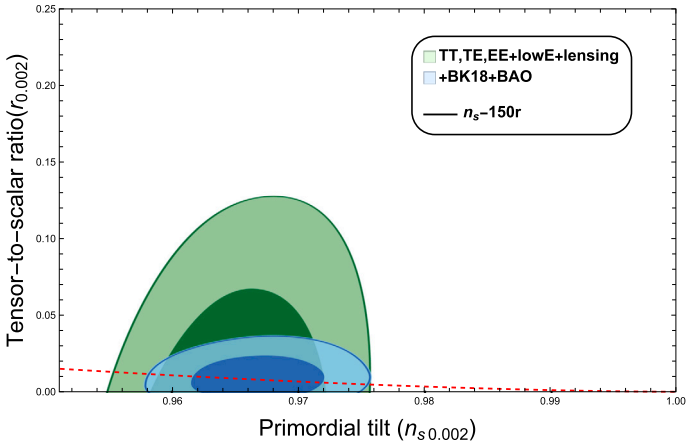

Fig. 8. Plot of r versus n_s for D-Brane ($p=4$) model.

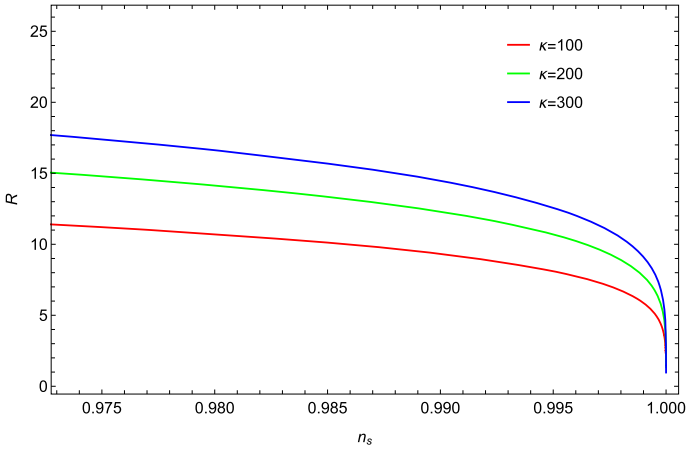

Fig. 9. Plot of R versus n_s for D-Brane ($p=4$) model with $a=1$.

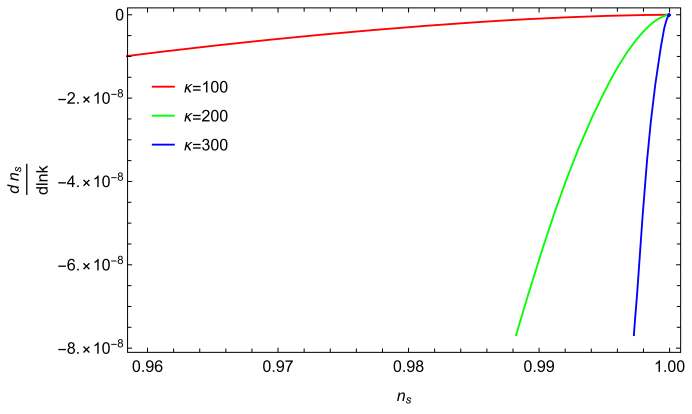

Fig. 10. Plot of $\frac{dn_s}{d\ln k}$ versus n_s for D-Brane ($p=4$) model with $a=0$.

validity. Fig. 11 ($a=1$) exhibits a characteristic decreasing trend for $n_s > 0.92$, with $\frac{dn_s}{d\ln k} \in [0.0000, 0.0006]$. While positive, this minimal running remains observationally permissible. Fig. 12 ($a=-1$) shows particularly compelling agreement with Planck data [53,54], as $\lim_{n_s \to 0.965} \Rightarrow \frac{dn_s}{d\ln k} \approx 0$. This asymptotic behavior matches precision CMB measurements.

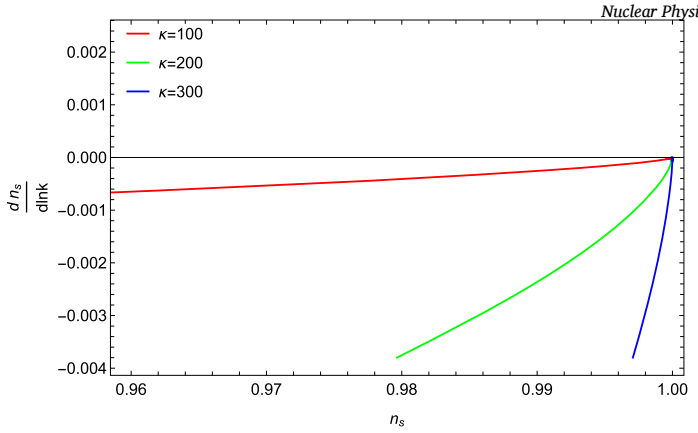

Fig. 11. Plot of $\frac{dn_s}{d\ln k}$ versus n_s for D-Brane ($p=4$) model with $a=1$.

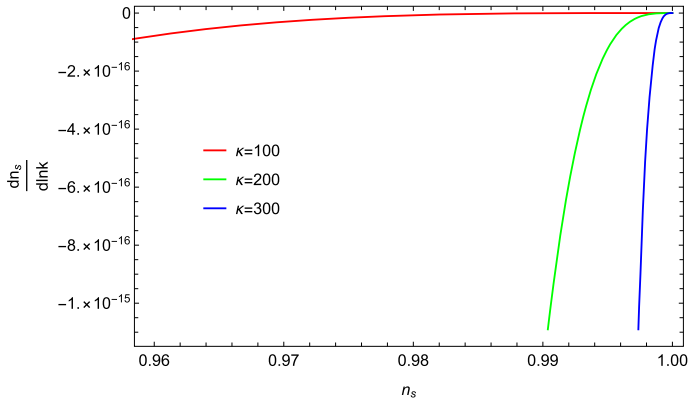

Fig. 12. Plot of $\frac{dn_s}{d\ln k}$ versus n_s for D-Brane ($p=4$) model with $a=-1$.

5. Potential with exponential tails model

Exponential potentials are characterized by inherent power-law dynamics, making them particularly advantageous for cosmological modeling due to their mathematically tractable form. This property enables closed-form solutions and reduces computational complexity in inflationary studies [47]. Their functional simplicity streamlines the analysis of inflationary evolution and its observational signatures. Motivated by these benefits, we adopt a single-field exponential potential of the form [43]

$$V = \Lambda^4\left(1 - e^{-\kappa q\phi}\right).$$

Within this scalar field configuration, the analysis extends to scenarios where the dissipative ratio significantly exceeds unity $R \gg 1$ and finds the same previous inflationary parameters.

5.1. Graphical part

- **Behavior of r Vs n_s:** Fig. 13 illustrates the parametric relationship between the tensor-to-scalar ratio (r) and the scalar spectral index n_s, analyzed across incremental variations in the parameter κ. The trajectories align with Planck 2018 constraints [53, 54], demonstrating theoretical consistency with observational bounds. Notably, all calculated values of r remain below the observational upper limit of $r < 0.066$ for scalar spectral indices within the observationally allowed range, further validating the model's compatibility with current cosmological datasets.

- **Behavior of R versus n_s:** Fig. 14 presents a systematic investigation of how the dissipative ratio R varies with the scalar spectral index n_s across different values of the dissipation parameter κ. Our analysis focuses on the observationally constrained range $0.94 \lesssim n_s \lesssim 0.99$, corresponding to the 68% confidence limits from precision CMB measurements. The results demonstrate that the range of R satisfying observational data sets.

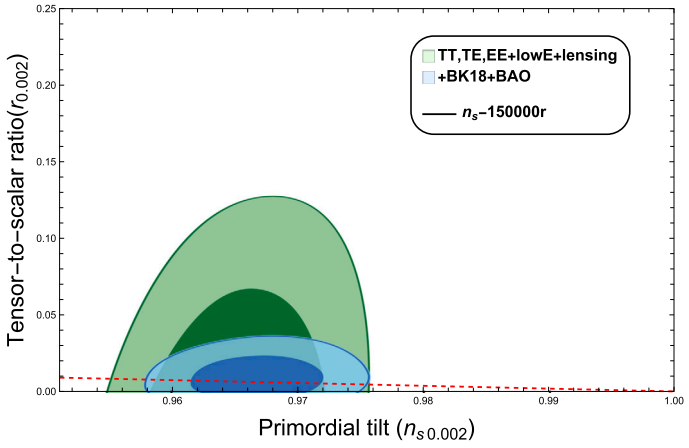

Fig. 13. Plot of r versus n_s for exponential tails potential.

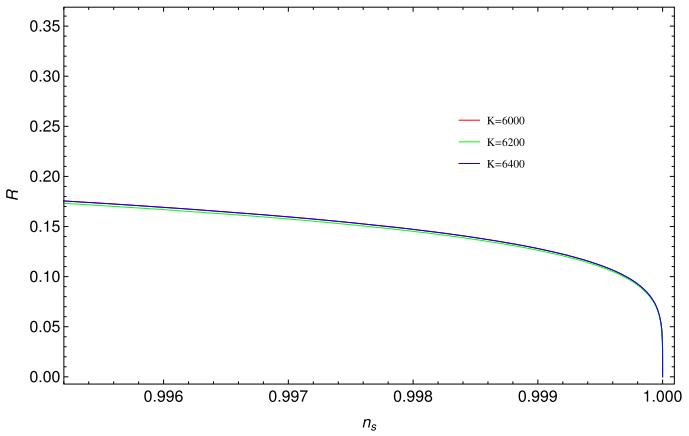

Fig. 14. Plot of R versus n_s for exponential tails potential with $a = 1$.

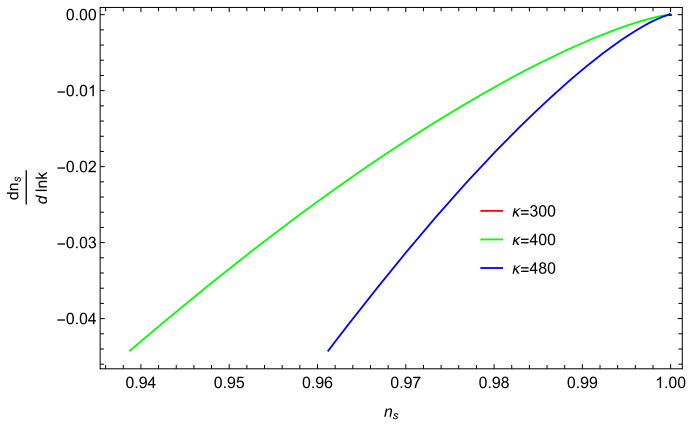

Fig. 15. Plot of $\frac{dn_s}{d\ln k}$ versus n_s for exponential tails potential with $a = 0$.

- **Behavior of $\frac{dn_s}{d\ln k}$ versus n_s:** Figs. 15–17 analyze the correlation between $\frac{dn_s}{d\ln k}$ and n_s for three distinct values of parameter a. For $a = 0$ (Fig. 15), the scalar spectral index spans $0.94 \leq n_s \leq 1.00$, while the running $\frac{dn_s}{d\ln k}$ occupies a narrow range of $-0.00015 \leq \frac{dn_s}{d\ln k} \leq 0$. The marginally negative values of $\frac{dn_s}{d\ln k}$ support consistency with modern observational constraints. For

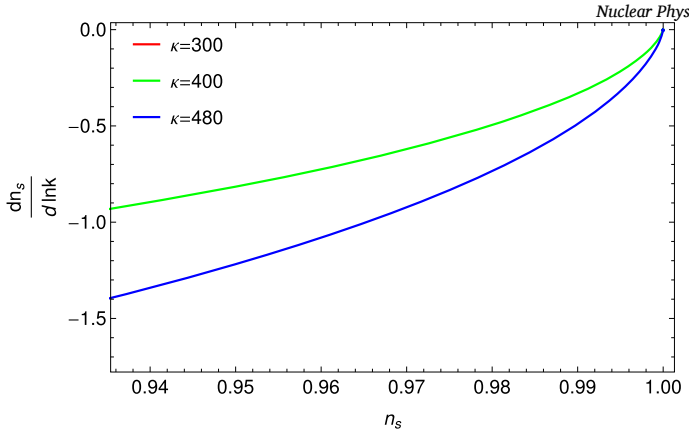

Fig. 16. Plot of $\frac{dn_s}{d\ln k}$ versus n_s for exponential tails potential with $a = 1$.

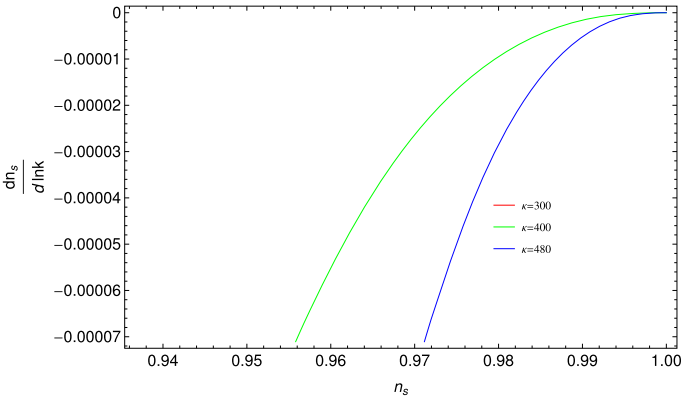

Fig. 17. Plot of $\frac{dn_s}{d\ln k}$ versus n_s for exponential tails potential with $a = -1$.

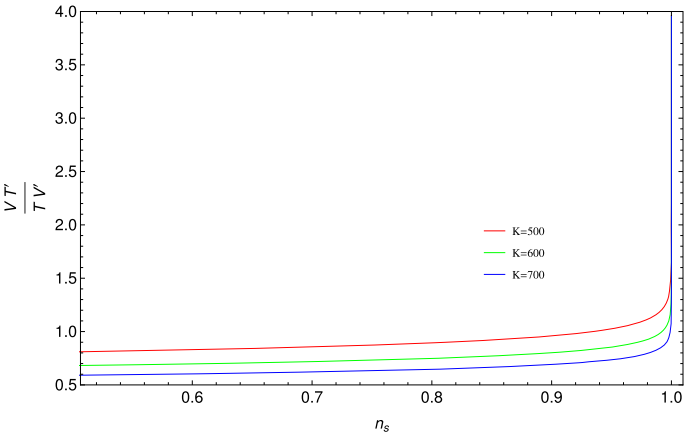

Fig. 18. Plot of $\frac{VT'}{TV'}$ versus n_s for exponential tails potential with $a = 0$.

$a = 1$ (Fig. 16), the running spans $-0.00015 \lesssim \frac{dn_s}{d\ln k} \lesssim 0.00007$, while $a = -1$ (Fig. 17) yields $-0.0005 \lesssim \frac{dn_s}{d\ln k} \lesssim 0$. These results exhibit slight negative deviations in $\frac{dn_s}{d\ln k}$, corroborating the Planck collaboration's bounds on inflationary dynamics [53,54].

- **Behavior of $\frac{VT'}{TV'}$ versus n_s:** Fig. 18 analyzes the correlation between the dimensionless parameter $\frac{VT'}{TV'}$, central to the de Sitter conjecture, and the scalar spectral index n_s, evaluated for three distinct values of κ. The analysis confirms that $\frac{VT'}{TV'} < 1$ across all tested scenarios, thereby supporting the theoretical bounds imposed by the swampland conjectures. This inequality aligns

with the conjectures' requirement for viable low-energy effective theories to avoid de Sitter-like vacua, further reinforcing the consistency of our framework with quantum gravity constraints.

6. Concluding remarks

In this study, we explore the dynamics of power-law plateau inflation within the warm inflation framework, drawing theoretical inspiration from GCG models. We employ a generalized dissipative coefficient, $\Gamma(\phi,T)=C_{\phi}\frac{T^{a}}{\phi^{a-1}}$. For underlying framework, we consider three plateau-type potentials: $V=\Lambda^{4}\left(1-\left(\frac{m}{\kappa\phi}\right)^{2}\right)$ (D-Brane model for $p=2$), $V=\Lambda^{4}\left(1-\left(\frac{m}{\kappa\phi}\right)^{4}\right)$ (D-Brane model for $p=4$) and $V=\Lambda^{4}(1-e^{-\kappa q\phi})$ (Potential with Exponential Tails model), each representing unique dissipative dynamics examined in prior literature. Our analysis centers on ($R\gg 1$), where thermal fluctuations dominate over quantum effects. We utilize slow-roll parameters to derive both the background evolution equations and perturbative observables, enabling a comprehensive examination of the interplay between dissipation, potential structure, and observational signatures. This approach allows us to systematically evaluate the consistency of these models with theoretical constraints and observational data, particularly in the context of the swampland conjectures and Planck collaboration bounds.

Our comprehensive calculations of key inflationary observables—including the scalar power spectrum $\mathcal{P}_{\mathcal{R}}$, spectral index n_s, its running $\frac{dn_s}{d\ln k}$, dissipative ratio R and the thermal stability parameter $\frac{T'V}{TV'}$—demonstrate remarkable consistency with current observational constraints. For every potential we examined, the results align precisely with Planck's latest measurements: the tensor-to-scalar ratio remains below $r<0.066$, the spectral index falls within $n_s=0.9661\pm0.0040$ and the running of the spectral index is consistent with $\frac{dn_s}{d\ln k}=-0.006\pm0.013$ [53,54]. Of particular significance is our finding that the ratio $\frac{T'V}{TV'}$, which tests the swampland conjectures, consistently takes values between 0 and 1 across all cases. This bounded range provides strong evidence that our model satisfies both string-theoretic consistency conditions and thermodynamic stability requirements during inflation. The robust agreement between our theoretical predictions and observational data, combined with the natural fulfillment of swampland criteria, suggests that warm inflation scenarios with strong dissipation effects may offer a compelling framework that bridges high-energy physics and cosmological phenomenology.

CRediT authorship contribution statement

Shama Sadiq: Writing – original draft, Visualization, Software, Investigation, Conceptualization. **Nadeem Azhar:** Writing – original draft, Visualization, Software, Investigation, Conceptualization. **N. Myrzakulov:** Visualization, Software, Investigation. **S. Toktarbay:** Visualization, Software, Investigation. **A. Muratkhan:** Visualization, Software, Investigation. **Sanjar Shaymatov:** Visualization, Software, Investigation. **Abdul Jawad:** Writing – review & editing, Writing – original draft, Validation, Software, Investigation, Conceptualization.

Declaration of competing interest

There are no conflicts of interest among the author.

Acknowledgements

This research is funded by the Science Committee of the Ministry of Science and Higher Education of the Republic of Kazakhstan (Grant No. AP23489541).

Data availability

No data was used for the research described in the article.

References

[1] A.G. Riess, Nat. Rev. Phys. 2 (2020) 10–12.
[2] A.G. Riess, et al., Astron. J. 116 (1998) 1009;
S. Perlmutter, et al., Astrophys. J. 517 (1999) 565.
[3] C.R. Contaldi, H. Hoekstra, A. Lewis, Phys. Rev. Lett. 90 (2003) 221303.
[4] D.N. Spergel, et al., Astrophys. J. Suppl. Ser. 148 (2003) 175;
D.N. Spergel, et al., Astrophys. J. Suppl. Ser. 170 (2007) 377.
[5] V. Sahni, A.A. Starobinsky, Int. J. Mod. Phys. D 9 (2000) 373;
S. Weinberg, Rev. Mod. Phys. 61 (1989) 1;
K. Bamba, S. Capozziello, S. Nojiri, S.D. Odintsov, Astrophys. Space Sci. 342 (2012) 155.
[6] A.A. Starobinsky, Phys. Lett. B 91 (1980) 99.
[7] A. Guth, Phys. Rev. D 23 (1981) 347.
[8] S. Han, W. Sun, B. Xiong, J. Phys. 75 (2003) 012001.
[9] Y. Hu, M.S. Turner, E.J. Weinberg, Phys. Rev. D 49 (1994) 3830–3836.

[10] A.D. Linde, Rep. Prog. Phys. 47 (1984) 925–986.
[11] A. Berera, Gravit. Cosmol. 11 (2005) 51–61.
[12] A. Hernandez-Almada, J. Magana, M.A. Garcia-Aspeitia, V. Motta, Eur. Phys. J. C 79 (2019) 22.
[13] A. Jawad, S. Maqsood, N. Azhar, M.M. Alam, Phys. Dark Universe 46 (2024) 101680;
A. Jawad, N. Azhar, S. Sadiq, S. Rani, Chin. Phys. C 48 (2024) 095107;
A. Jawad, A.M. Sultan, N. Azhar, Mod. Phys. Lett. A 37 (2022) 2250166;
A. Jawad, S. Rani, K. Bamba, N. Azhar, Mod. Phys. Lett. A 35 (2020) 2050268.
[14] M. Motaharfar, V. Kamali, R.O. Ramos, Phys. Rev. D 99 (2019) 063513.
[15] S. Ebrahimi, K. Vahid, A. Asma, Eur. Phys. J. C 81 (2021) 19.
[16] S. Rani, A. Jawad, A.M. Sultan, A. Majeed, Int. J. Mod. Phys. D 32 (2023) 2350004.
[17] S. Chaplygin, Trans. by M. Slud, Brown University, 1944.
[18] M.R. Setare, Phys. Lett. B 648 (2007) 329.
[19] K. Bamba, et al., Astrophys. Space Sci. 342 (2012) 155.
[20] P. Saha, U. Debnath, Eur. Phys. J. C 79 (2019) 919;
S. Sahlu, et al., Eur. Phys. J. C 79 (2019) 749;
M. Jamil, M.A. Rashid, Eur. Phys. J. C 58 (2008) 111–114.
[21] R. Bean, O. Dore, Phys. Rev. D 68 (2003) 023515;
H. Sandvik, et al., Phys. Rev. D 69 (2004) 123524.
[22] M.C. Bento, O. Bertolami, A.A. Sen, Phys. Rev. D 66 (2002) 043507.
[23] M.C. Bento, O. Bertolami, A.A. Sen, Phys. Rev. D 70 (2004) 083519.
[24] M. Bastero-Gill, A. Berera, Phys. Rev. D 72 (2005) 103526.
[25] M.R. Setare, Phys. Lett. B 648 (2007) 329.
[26] K. Bamba, Math. Phys. 09 (2018) 50–59.
[27] K. Bamba, et al., Phys. Rev. D 90 (2014) 124061.
[28] S. Nojiri, S.D. Odintsov, E.N. Saridakis, Phys. Lett. B 797 (2019) 134829.
[29] K. Bamba, S.D. Odintsov, Symmetry 7 (2015) 220.
[30] K. Bamba, S. Capozziello, S. Nojiri, S.D. Odintsov, Astrophys. Space Sci. 342 (2012) 155.
[31] A. Jawad, A. Ilyas, S. Rani, Astropart. Phys. 81 (2016) 61–71.
[32] A. Jawad, S. Butt, S. Rani, Eur. Phys. J. C 76 (2016) 274.
[33] A. Jawad, S. Chaudhary, N. Videla, Eur. Phys. J. C 77 (2017) 808.
[34] A. Jawad, et al., Eur. Phys. J. C 77 (2017) 700.
[35] A. Jawad, N. Videla, F. Gulshan, Eur. Phys. J. C 77 (2017) 271.
[36] A. Jawad, A. Ilyas, S. Rani, Eur. Phys. J. C 77 (2017) 131.
[37] A. Jawad, S. Chaudhary, Int. J. Mod. Phys. D 27 (2018) 1850087.
[38] A. Jawad, A. Rustam, Astropart. Phys. 11 (2020) 102402.
[39] J. Sadeghi, S. Noori Gashti, Eur. Phys. J. C 81 (2021) 1–10.
[40] S. Noori Gashti, J. Hologr. Appl. Phys. 2 (1) (2022) 13–24.
[41] S. Noori Gashti, J. Sadeghi, Int. J. Mod. Phys. A 37 (04) (2022) 2250006.
[42] S. Noori Gashti, J. Sadeghi, B. Pourhassan, Astropart. Phys. 139 (2022) 102703.
[43] J. Martin, C. Ringeval, V. Vennin, Phys. Dark Universe 56 (2014) 29.
[44] O. Bertolami, V. Duvvuri, Phys. Lett. B 640 (2006) 121.
[45] D.J.H. Chung, G. Shiu, M. Trodden, Phys. Rev. D 68 (2003) 063501.
[46] N. Videla, G. Panotopoulos, Phys. Rev. D 97 (2018) 123503.
[47] Y. Akrami, et al., Astron. Astrophys. 644 (2020) A99.
[48] C. Vafa, arXiv:hep-th/0509212, 2005.
[49] G. Obied, H. Ooguri, L. Spodyneiko, C. Vafa, arXiv:1806.08362, 2018.
[50] H. Ooguri, E. Palti, G. Shiu, C. Vafa, Phys. Lett. B 788 (2019) 180.
[51] S.K. Garg, C. Krishnan, J. High Energy Phys. 11 (2019) 075.
[52] R. Brandenberger, V. Kamali, R.O. Ramos, J. High Energy Phys. 2020 (2020) 127.
[53] N. Aghanim, et al., Astron. Astrophys. 641 (2020) A6.
[54] N. Aghanim, et al., Astron. Astrophys. 641 (2020) A10.